High-temperature thermochemical energy storage based on redox reactions using Co-Fe and Mn-Fe mixed metal oxides

Laurie André, Stéphane Abanades, Laurent Cassayre

▶ **To cite this version:**

Laurie André, Stéphane Abanades, Laurent Cassayre. High-temperature thermochemical energy storage based on redox reactions using Co-Fe and Mn-Fe mixed metal oxides. Journal of Solid State Chemistry, 2017, 253, pp.6 - 14. 10.1016/j.jssc.2017.05.015 . hal-01786111

HAL Id: hal-01786111
https://hal.science/hal-01786111

Submitted on 20 Jul 2018

HAL is a multi-disciplinary open access archive for the deposit and dissemination of scientific research documents, whether they are published or not. The documents may come from teaching and research institutions in France or abroad, or from public or private research centers.

L'archive ouverte pluridisciplinaire **HAL**, est destinée au dépôt et à la diffusion de documents scientifiques de niveau recherche, publiés ou non, émanant des établissements d'enseignement et de recherche français ou étrangers, des laboratoires publics ou privés.

OATAO
Open Archive Toulouse Archive Ouverte

Open Archive Toulouse Archive Ouverte

OATAO is an open access repository that collects the work of Toulouse researchers and makes it freely available over the web where possible

This is an author's version published in: http://oatao.univ-toulouse.fr/20472

Official URL : http://doi.org/10.1016/j.jssc.2017.05.015

To cite this version: André, Laurie and Abanades, Stéphane and Cassayre, Laurent *High-temperature thermochemical energy storage based on redox reactions using Co-Fe and Mn-Fe mixed metal oxides.* (2017) Journal of Solid State Chemistry, 253. 6-14. ISSN 0022-4596

Any correspondence concerning this service should be sent to the repository administrator: tech-oatao@listes-diff.inp-toulouse.fr

High-temperature thermochemical energy storage based on redox reactions using Co-Fe and Mn-Fe mixed metal oxides

Laurie André[a], Stéphane Abanades[a,*], Laurent Cassayre[b]

[a] *Processes, Materials, and Solar Energy Laboratory, PROMES-CNRS, 7 Rue du Four Solaire, 66120 Font-Romeu, France*
[b] *Laboratoire de Génie Chimique, Université de Toulouse, CNRS, INPT, UPS, Toulouse, France*

Keywords:
Metal oxide
Thermal heat storage
Solid-gas reaction
Reduction
Oxidation
Thermodynamic equilibrium calculations

A B S T R A C T

Metal oxides are potential materials for thermochemical heat storage via reversible endothermal/exothermal redox reactions, and among them, cobalt oxide and manganese oxide are attracting attention. The synthesis of mixed oxides is considered as a way to answer the drawbacks of pure metal oxides, such as slow reaction kinetics, loss-in-capacity over cycles or sintering issues, and the materials potential for thermochemical heat storage application needs to be assessed. This work proposes a study combining thermodynamic calculations and experimental measurements by simultaneous thermogravimetric analysis and calorimetry, in order to identify the impact of iron oxide addition to Co and Mn-based oxides. Fe addition decreased the redox activity and energy storage capacity of Co_3O_4/CoO, whereas the reaction rate, reversibility and cycling stability of Mn_2O_3/Mn_3O_4 was significantly enhanced with added Fe amounts above ~15 mol%, and the energy storage capacity was slightly improved. The formation of a reactive cubic spinel explained the improved re-oxidation yield of Mn-based oxides that could be cycled between bixbyite and cubic spinel phases, whereas a low reactive tetragonal spinel phase showing poor re-oxidation was formed below 15 mol% Fe. Thermodynamic equilibrium calculations predict accurately the behavior of both systems. The possibility to identify other suitable mixed oxides becomes conceivable, by enabling the selection of transition metal additives for tuning the redox properties of mixed metal oxides destined for thermochemical energy storage applications.

1. Introduction

The purpose of thermal energy storage (TES) in solar thermal power plants is to store solar heat in the form of sensible, latent or chemical energy during on-sun hours and then to use it during off-sun hours in order to match a variable electricity demand with an intermittent energy source supply, thus enabling energy production according to needs and enhancing energy generation dispatchability [1]. This study focuses on thermochemical heat storage, which shows advantages over latent and sensible heat storage, including higher energy storage densities, possible heat storage at room temperature in the form of stable solid materials, and long term storage in a broad temperature range (400–1200 °C) with heat released at a constant restitution temperature defined by the reaction equilibrium. Concentrated solar power (CSP) provides the heat source required for endothermal/exothermal reversible reactions involved in thermochemical energy storage (Eqs. (1) and (2)) in order to store solar energy in the form of chemical bonds. When combined with CSP systems, the continuous production of electricity in thermal power plants becomes possible. The reaction enthalpy is stored in the reaction products during the heat charge (Eq. (1)), and can be released by reversing the reaction during the discharge (Eq. (2)).

$$MO_{(ox)} + \text{Heat} \rightarrow MO_{(red)} + \alpha\ O_{2(g)} \quad (1)$$

$$MO_{(red)} + \alpha\ O_{2(g)} \rightarrow MO_{(ox)} + \text{Heat} \quad (2)$$

An advantage of using metal oxides as TES materials is the use of air as the heat transfer fluid that can be processed in an open-loop system. Such thermochemical systems are suitable for application in high-temperature solar power plants based on central air receiver (pressurized air-based solar tower receivers for power generation via gas turbines). Cobalt oxide (Co_3O_4) and manganese oxide (Mn_2O_3), which reduce into CoO and Mn_3O_4 respectively, are among the most studied metal oxides considered as promising materials for thermochemical energy storage. Experiments showed that Co_3O_4 is the most suited raw material given the fast reaction kinetics, complete reaction reversibility and cycling stability with a measured gravimetric energy storage density of 576 kJ/kg [2] (while reported theoretical enthalpy is

* Corresponding author.
E-mail address: stephane.abanades@promes.cnrs.fr (S. Abanades).

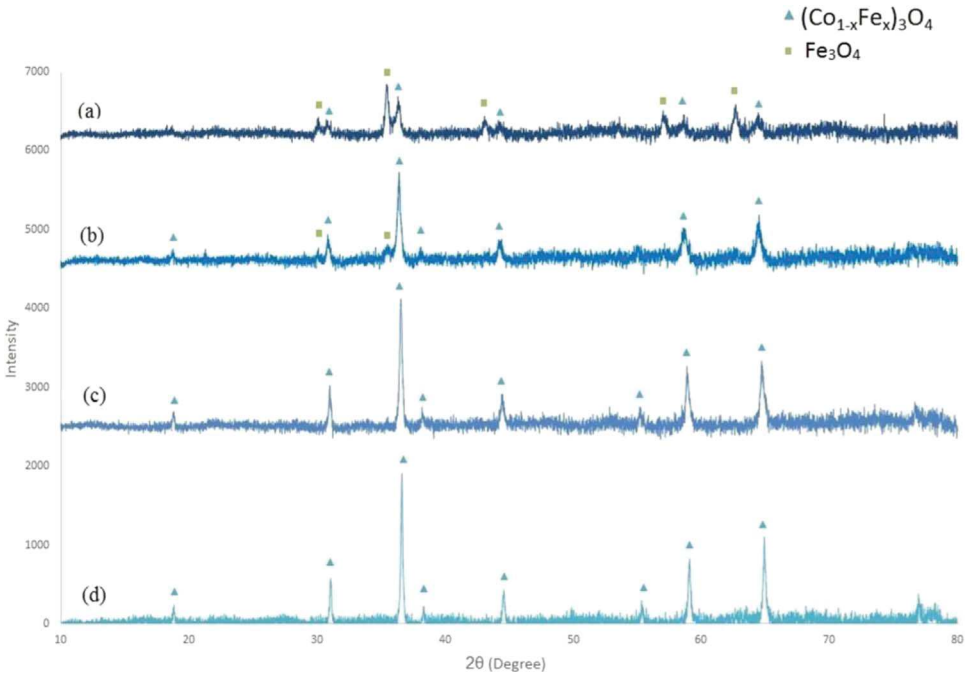

Fig. 1. XRD analysis of fresh synthetic Co_3O_4 with (a) 40 mol% Fe, (b) 25 mol% Fe, (c) 10 mol% Fe, and (d) 5 mol% Fe.

844 kJ/kg [3–6]). However, the cost and potential toxicity of cobalt oxide may require the development of other alternative materials. The reduction step of Mn_2O_3 was observed in the range of 920–1000 °C, with notably slow re-oxidation in the range of 850–500 °C, with a reported gravimetric energy storage density of 110–160 kJ/kg [7,8] and a theoretical enthalpy of 202 kJ/kg [8]. The re-oxidation usually happens in two steps, the first one being during the cooling and in between 700 °C and 500 °C and the second one being during the re-heating and in the range of 500–850 °C [9] because of strong kinetic limitations. In order to complete the slow re-oxidation during the cooling step, it needs to last long enough by decreasing drastically the cooling rate.

Optimization of materials reactivity is generally required for metal oxide species by using e.g. doping strategies, controlled synthesis techniques for tailored morphology, or stabilization with inert materials to alleviate sintering effects. Improvement of materials properties and flexibility such as reaction kinetics and reaction temperature tuning can be obtained by the addition of dopants. In the specific case of the Mn_2O_3/Mn_3O_4 cycle, the doping with transition metals is an option to relieve the slow re-oxidation issue [2,4].

The present study aims at investigating the effect of Fe addition on the performances of Co and Mn metal oxides, which have been identified as interesting candidates for TES [10]. The optimal mixed metal oxide composition to reach the highest performances for TES is addressed, encompassing high reaction enthalpy, stability upon cycling, low temperature gap between reduction and re-oxidation, and reaction in a temperature range adapted to CSP. The addition of transition metals is investigated as a way to answer the drawbacks of simple metal oxides, including slow reaction kinetics [5], sintering [11], loss-in-capacity over cycles [8], etc. Block et al. [2] reported that both addition of iron to cobalt oxide or addition of cobalt to iron oxide results in lower enthalpies of reaction compared to those of the pure oxides. However, they estimated that cobalt oxide doped with 10% of iron possesses higher reduction/oxidation reversibility than pure cobalt oxide and still shows high enthalpy of reaction. Pagkoura et al. [9] showed that cobalt oxide with 10–20 wt% of iron shows good thermo-mechanical stability over ten redox cycles. Carrillo et al. [11] showed that the addition of iron does not allow avoiding the sintering encountered with Mn_2O_3 but helps to increase the heat storage density of the material. Furthermore, the addition of iron helped to stabilize and enhance the oxidation rate of manganese oxide over thirty redox cycles. According to their study, the fastest and most stable oxidation reaction was obtained for Mn_2O_3 doped with 20 mol% Fe. In another study, the authors also considered Fe-Cu co-doping in manganese oxide and showed that the incorporation of Cu diminished the reduction temperature, whereas the incorporation of Fe increased the oxidation temperature [12].

Recent models provide thermodynamic descriptions of the Co-Fe-O [13,14] and Mn-Fe-O [15,16] systems, based on exhaustive studies of available experimental data. In the present work, some of these models were used to calculate the nature and composition of solid phases at equilibrium, the oxygen storage capacity (equal to the mass loss during reduction), the transition temperature, and the reaction enthalpy of Co-Fe and Mn-Fe mixed oxides, with Fe content up to 50 mol%. Equilibrium calculations were compared to experimental (thermogravimetric and calorimetric) measurements carried out with various oxide compositions, under 20%O_2/Ar atmosphere, in the 750–1050 °C temperature range. The combination of experimental data and thermodynamics aims at providing a better understanding of the behavior of the mixed oxides and defining the optimal composition.

2. Materials and methods

2.1. Synthesis and characterization

Pure Co_3O_4 and cobalt oxide mixed with 5, 10, 25, and 40 mol% Fe as well as pure Mn_2O_3 and manganese oxide mixed with 10, 15, 20, 30, 40 and 50 mol% Fe were synthesized. In the following, the oxides compositions are either noted x(Fe) or mol% Fe, referring to the molar content of Fe on metal basis (based on a Fe/(Fe+Co) and Fe/(Fe+Mn) mole ratio). All the powders were synthesized via a modified Pechini method [2], using metal nitrates (> 98% purity), citric acid (> 99% purity) and ethylene glycol (> 99% purity) in aqueous solution. The solution was heated up until obtaining a viscous solution. The powders were then calcined in air at 200 °C for 2 h and at 750 °C for 4 h in order to fully eliminate the organic fraction and residues of the synthesis, and to stabilize the structure. Higher calcination temperatures were not considered to avoid the reduction of the materials during the synthesis.

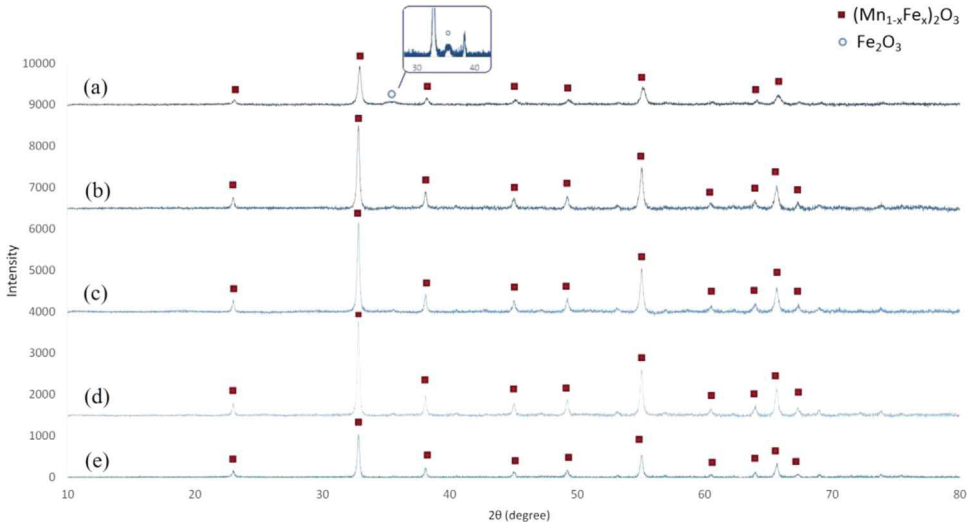

Fig. 2. XRD analysis of fresh synthetic Mn_2O_3 with (a) 50 mol% Fe, (b) 40 mol% Fe, (c) 30 mol% Fe, (d) 20 mol% Fe, and (e) 10 mol% Fe.

The powders were characterized by X-ray diffraction (XRD) before being studied in redox cycles. XRD analysis was performed (Figs. 1 and 2, SI1, SI2) at room temperature using a PANalytical XPert Pro diffractometer (CuKα radiation, λ = 0.15418 nm). X-ray diffraction measurements of θ-θ symmetrical scans were made over an angular range of 10–80°. The step size and the time per step were fixed at 0.01° and 20 s, respectively. The contribution from $K\alpha_2$ was removed and the X-ray diffractograms were recorded and studied using the PANalytical software. The instrumental function was determined using a reference material (SRM 660, lanthanum hexaboride, LaB_6 polycrystalline sample) and can be expressed by a polynomial function [17]. The synthesized oxide phases were corresponding to the structures of (i) a cubic spinel solution $(Co_{1-x}Fe_x)_3O_4$ (Fig. 1) and (ii) a bixbyite solution $(Mn_{1-x}Fe_x)_2O_3$ [18] (Fig. 2), with traces of iron oxide only detected for the materials containing the largest amount of iron (Figs. 1a and b, and 2a). Above 20 mol% Fe added to Co_3O_4, the material is no longer a single spinel phase but a mixture of two spinels.

The morphology of the synthesized $(Mn_{1-x}Fe_x)_2O_3$ phase was also characterized (Fig. SI3) by SEM (FESEM, HITACHI S4800). The very porous structure obtained with the Pechini method can be observed in Mn_2O_3 samples synthesized with no iron (Fig. SI3a and b). The porous structure is still present with the addition of iron during the synthesis; however, the porosity reduces with increasing iron content. The sample with 10 mol% Fe (Fig. SI3c and d) still resembles the pure Mn_2O_3 sample, while the sample with 50 mol% Fe appears different (Fig. SI3e and f), with thicker necks forming the pore walls. This change in morphology does not alter the reactivity, as evidenced in the experimental section.

2.2. Experimental procedure for thermochemical redox cycling

Experimental data concerning transition temperatures during redox process, oxygen storage capacity and reaction enthalpies were obtained by coupled thermogravimetric analysis (TGA) and differential scanning calorimetry (DSC), using a Netzsch STA 449 F3 System. About 50 mg of powder was placed into an alumina crucible and then subjected to simultaneous thermal analysis (STA) consisting of TGA coupled with DSC.

Reduction-oxidation cycles were performed in a 20% O_2/Ar atmosphere (10 N mL/min O_2 and 40 N mL/min Ar), between 800 °C and 1050 °C for cobalt based oxides and between 750 °C and 1050 °C for manganese based oxides. Each run also included a last reduction step under Ar (99.999% purity), in order to get information about the reduction temperature of the material under inert atmosphere. The heating rate was 20 °C/min for the reduction step, and the cooling rate was 10 °C/min for the re-oxidation step. For some runs with cobalt based oxides, the temperature was maintained for 15 min at 1050 °C and at 800 °C for achieving the state of reaction equilibrium. For all the materials, a series of three cycles was performed for each studied formulation in order to determine their suitability for achieving reversible reactions and to assess a possible chemical deactivation of the materials as a result of a loss of redox stability during thermal treatment.

2.3. Thermodynamic calculations

Equilibrium calculations were performed with the FactSage 7.0 software [19] and the FToxid database, which includes models of the thermochemical properties of the oxide phases in Fe-Co-O [13] and Fe-Mn-O [15] systems. For calculations in the Fe-Co-O system, the following solid phases were considered: the Fe_2O_3 compound, the cubic spinel solution $(Co_{1-x}Fe_x)_3O_4$ (C-Spin) and the monoxide solution $(Co_{1-x}Fe_x)O_{1+y}$ (Monoxide). For the Fe-Mn-O systems, four phases were considered: two spinel solutions $(Mn_{1-x}Fe_x)_3O_4$, one with cubic structure (C-Spin) and the other with tetragonal structure (T-Spin), the bixbyite solution $(Mn_{1-x}Fe_x)_2O_3$ (Bixb) and the corundum solution $(Fe_{1-x}Mn_x)_2O_3$ (Cor). The monoxide and spinel solid solutions were described within the framework of the Compound Energy Formalism [20], with two and three ionic sublattices, respectively (see [13,15] for more details). The bixbyite and corundum phases were modelled as a random mixture of the two end-members (Fe_2O_3 and Mn_2O_3), with no interaction parameter [15]. Two gaseous components, O_2 and Ar, were taken into account, with ideal mixing properties. The total pressure was always 1 atm.

For both systems, two kinds of calculations were carried out: (i) plot of phase diagrams, (ii) system equilibrium at various compositions and temperatures, providing, for each composition and at each temperature step, the phase assemblage and the cationic distribution in each solution phases, as well as the total enthalpy of the system.

The second type of calculations gives access to the theoretical mass loss (i.e. oxygen storage capacity), Δm, as defined by (Eq. (3)). This quantity is directly comparable to the mass change measured by TGA.

$$\Delta m\ (\%) = 100.\frac{mass\ of\ solid\ at\ T_{max} - mass\ of\ solid\ at\ T_{min}}{mass\ of\ solid\ at\ T_{min}} \quad (3)$$

where T_{min} and T_{max} are referring to the minimal and maximal temperature of the thermochemical cycle.

The enthalpy of the reduction reaction (Eq. (1)), $\Delta_r H$, was

calculated according to (Eq. (4)). This quantity is compared to the heat of reaction determined by DSC analysis. For reactions occurring on a large temperature range (see Section 3), this calculation includes a contribution due to the calorific capacity of the compounds (sensible heat), which leads to an overestimation of the enthalpy strictly related to the reaction.

$$\Delta_r H\ (\text{kJ/kg}\ \ of\ s^0) = \frac{1}{m_s{}^0}[m_s{}^1 H^{s^1}(T_{end}) + m_s{}^2 H^{s^2}(T_{end}) + m_{O2} H^{O2}(T_{end})] - H^{s^0}(T_{beg}) \quad (4)$$

where T_{end} is the temperature (°C) at the end of the phase transition or the maximal temperature of the cycle; T_{beg} is the temperature (°C) at the beginning of the phase transition; $m_S{}^0$ is the mass (kg) of the solid phase at T_{min}; $m_S{}^1$ and $m_S{}^2$ are the mass (kg) of the solid phases at T_{end}; m_{O2} is the mass (kg) of dioxygen at T_{end}; $H^x(T)$ is the enthalpy (kJ/kg) of the compound x at the temperature T.

3. Results and discussion

3.1. Cobalt-based mixed oxides

The calculated Co-Fe-O phase diagram for pO_2 = 0.20 atm is presented in Fig. 3a. It shows that, at equilibrium, the iron content greatly influences the composition and the amount of the monoxide phase formed at 1050 °C when heating the spinel phase from 800 °C. For small Fe additions (0 < x(Fe) < 0.1), the spinel phase is fully converted into the monoxide phase. At very high Fe content (x(Fe) > 0.6), there is no phase transition achievable below 1200 °C, which is the upper temperature limit usually considered for TES applications. For intermediate Fe content (0.1 < x(Fe) < 0.6), an increasing proportion of spinel phase is not converted into monoxide. As an example, Fig. 3b presents the influence of the temperature on the phases amount for x(Fe) = 0.25. A temperature of about 1460 °C is required to fully convert the spinel phase into the monoxide phase. Furthermore, as illustrated in Fig. 3c for x(Fe) = 0.25, the monoxide phase $(Co_{1-x}Fe_x)O_{1+y}$ presents a noticeable over-stoichiometry (y) in oxygen, which increases with temperature.

The TGAs of cobalt-based oxides are presented in Figs. 4 and 5 with different temperature programs. A first observation is that a noticeable change in the re-oxidation onset temperature (Fig. SI4) is measured between the samples with 0–10 mol% Fe (Figs. 4b–c, 5c–e) and with 25–40 mol% Fe (Figs. 4a, 5a–b). Indeed, the re-oxidation step starts at the beginning of the temperature decrease (i.e. 1050 °C) for the samples containing 25 mol% Fe and 40 mol% Fe, which is in line with the phase diagram (Fig. 3a) since the two-phase equilibrium strongly depends on the temperature. The Co-Fe samples were kept in a reduced state after TGA (final cooling step in Ar to avoid re-oxidation in Fig. 5) and analysed via XRD (Fig. SI1). Phase identification confirmed the presence of the single monoxide phase for low Fe contents (0 and 5 mol %), whereas the samples consisted of a mixture of monoxide and spinel phases for higher Fe contents (10–40 mol%), in agreement with the calculated phase diagram.

The influence of Fe incorporation on reaction temperatures is reported in Fig. 6 (Fig. SI4 compares data under Ar and 20%O_2/Ar atmosphere). Both temperatures at peak reaction rate (i.e. temperatures at which the reaction kinetics reached its maximum, Fig. 6) and onset temperatures (Fig. SI4) were measured. The measured onset temperature for reduction of Co_3O_4 to CoO is about 920 °C, which is in good accordance with previous studies carried out in air atmosphere, reporting temperatures ranging from 880 to 930 °C [6,7,9,21]. A gradual increase of the reduction and oxidation temperatures is observed with increasing amount of iron in the material, which is consistent with the phase diagram (Fig. 3a). An effect of Fe addition on the temperature gap between reduction and oxidation is also evidenced. Indeed, as both temperatures rise with Fe addition, it can be noticed that the gap between the reduction and oxidation temperatures reduces. For 40 mol% Fe, the onset temperature for reduction has increased by 50 °C compared to pure Co_3O_4, while the onset temperature for oxidation has increased by 90 °C. The reduction of this temperature gap is an asset for large-scale applications since it reduces the amount of energy spent for the heating and cooling of the system between the charge and the discharge steps. However, an increase in the oxidation temperature may also be a disadvantage if the system must be externally heated to initiate the oxidation (in case the material is stored in reduced form at room temperature).

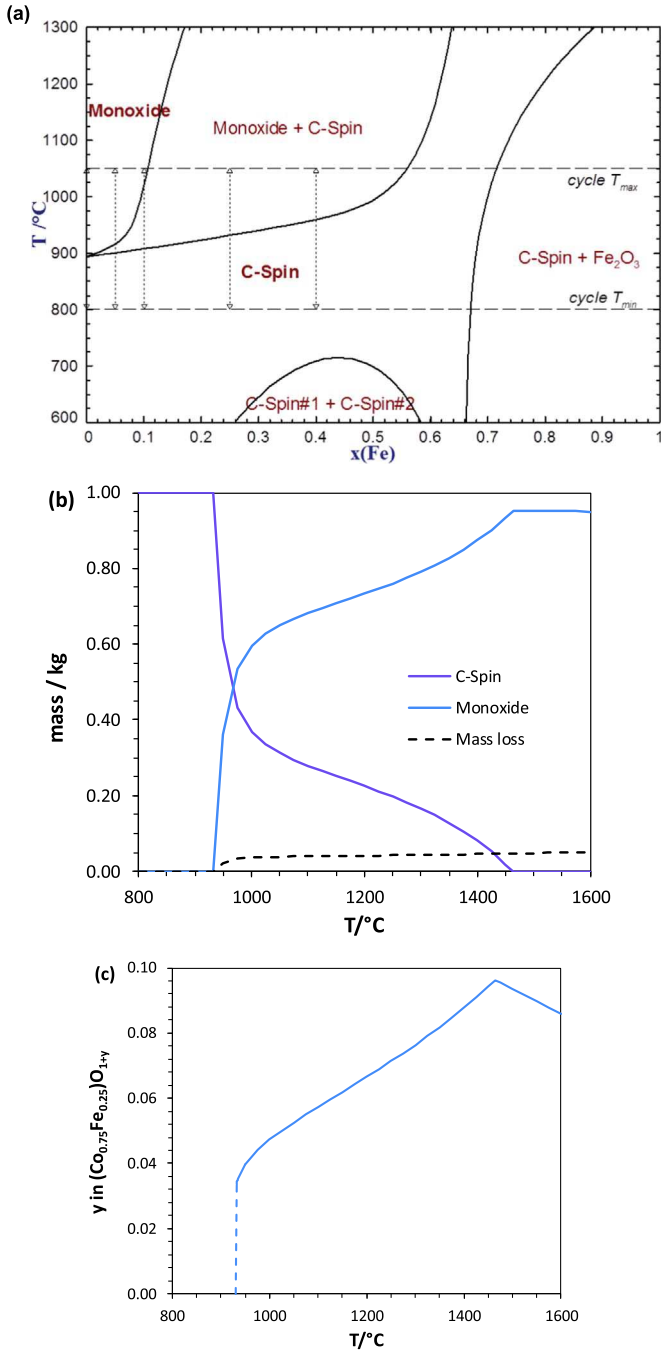

Fig. 3. (a) Calculated Co-Fe-O phase diagram at pO_2 = 0.20 atm, (b) calculated temperature evolution of the mass of solid phases for x(Fe) = 0.25, (c) calculated temperature evolution of oxygen over-stoichiometry (y) in the monoxide phase $(Co_{0.75}Fe_{0.25})O_{1+y}$.

In Fig. 7 are reported, along with the calculated equilibrium values,

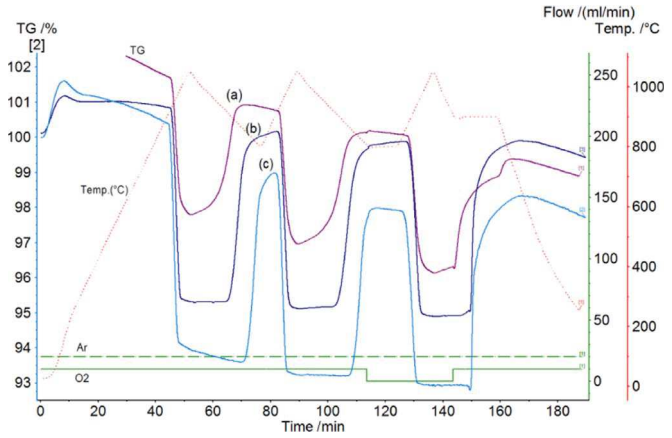

Fig. 4. TGA of Co_3O_4/CoO with addition of (a) 25 mol% Fe, (b) 10 mol% Fe, (c) 5 mol% Fe, including a final re-oxidation step under 20% O_2/Ar at the end.

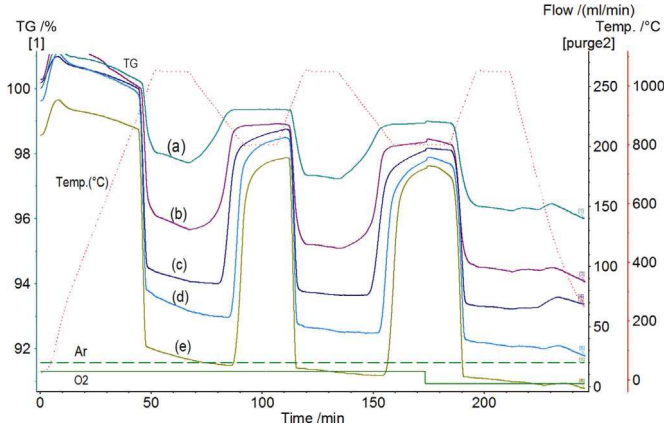

Fig. 5. TGA of Co_3O_4/CoO with addition of (a) 40 mol% Fe, (b) 25 mol% Fe, (c) 10 mol% Fe, (d) 5 mol% Fe, (e) no Fe added, ending on a final reduction step under Ar.

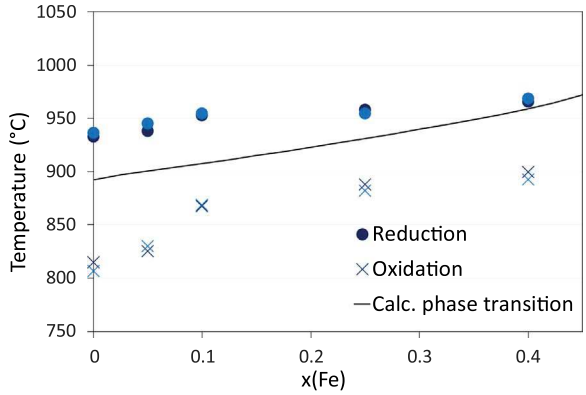

Fig. 6. Experimental temperatures at peak reaction rate for cobalt-based oxides in 20% O_2/Ar and comparison with the calculated temperature of the C-Spin/Monoxide transition.

the maximum values of Δm measured for each oxide composition, which means the highest amount of O_2 released during reduction, and the average Δm for the three redox cycles. The hypothetic case of a full conversion of the initial spinel into a stoichiometric monoxide, calculated according to (Eq. (5)), is also plotted in Fig. 7.

$$(Co_{1-x}Fe_x)_3O_{4(s)} = 3\,(Co_{1-x}Fe_x)O_{(s)} + 0.5\,O_2(g) \quad (5)$$

Measurements of the Δm values clearly show that increasing the amount of iron in the material reduces the amount of O_2 it is able to release at a given temperature. Furthermore, the maximum Δm values are in excellent accordance with equilibrium calculations, which

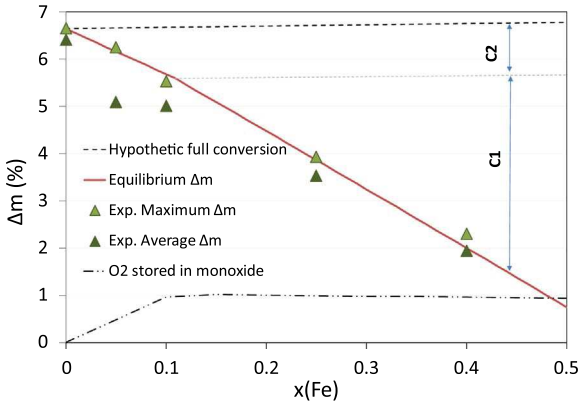

Fig. 7. Average and maximal experimental mass loss (Δm in %) of the Co-Fe mixed oxide between 800 °C and 1050 °C compared to Δm at thermodynamic equilibrium.

implies that a full conversion has been reached.

According to the thermodynamic model, the decrease in O_2 storage capacity with increasing Fe content is due to a combination of two factors. First, as evidenced by the phase diagram and the temperature profile for x(Fe) = 0.25 (Fig. 3b), the upper temperature limit of 1050 °C does not lead to a full conversion of the spinel phase when x(Fe) > 0.10. This contribution is represented as C1 in Fig. 7. It does not account for the decrease in Δm evidenced for x(Fe) = 0.05 and 0.10 (C2 in Fig. 7), which should be closer to the mass loss calculated according to (Eq. (5)) since a full conversion into monoxide occurs. This second factor is linked with the fact that the monoxide solid solution becomes non stoichiometric with the incorporation of Fe (Fig. 3c). This leads to a residual storage of oxygen in the monoxide phase, according to (Eq. (6)):

$$(Co_{1-x}Fe_x)_3O_{4(s)} = 3\,(Co_{1-x}Fe_x)O_{1+y(s)} + (1-3y)/2\,O_2(g) \quad (6)$$

where y is the over-stoichiometry of oxygen in the monoxide phase.

As illustrated in Fig. 7, the calculated contribution of the oxygen over-stoichiometry in the monoxide phase at 1050 °C accounts for a loss of storage capacity of about 1% per unit mass of spinel when x(Fe) > 0.10, as compared to a maximum capacity of 6.6% for pure cobalt oxide.

As for the cycling stability, for pure Co_3O_4, the average Δm is the same as both the theoretical value and the maximum value measured experimentally. This means that the amount of O_2 released and regained did not change, confirming the good material cycling stability over three cycles, as already reported by several authors [2–7]. For the samples containing 5 and 10 mol% iron, since the average Δm falls slightly below the theoretical and maximum value, a minor loss in O_2 exchange capacity upon cycling is evidenced. Conversely, the amount of O_2 exchanged remains stable over cycles for larger Fe contents (x(Fe) > 0.10) at the expense of a decreased oxygen storage capacity. Thus, the cycling stability of cobalt oxide does not suffer from the addition of iron, as the re-oxidation conversion rate is not significantly decreasing over multiple cycles for Co-Fe mixed oxides, similarly to pure Co_3O_4. An additional cycling test was performed with a Co-Fe mixed oxide (10 mol% Fe) subjected to multiple consecutive cycles (12 cycles) in order to demonstrate the stability of the material regarding both oxygen storage capacities and energy storage densities (Fig. SI5). This confirms the robustness of the active redox materials and the ability to cycle without deactivation.

Regarding the effect of the gas flow composition, the measured Δm due to the reduction under pure Ar was not significantly different from the one measured with 20% O_2/80% Ar. However, as illustrated by Fig. SI4, the reduction onset temperature under Ar was decreased by 60–80 °C, to reach a value of about 860 °C, almost independent of x(Fe). These data are rather different from the equilibrium state calculated with the thermodynamic model (Fig. SI6). Indeed, under pure Ar, the

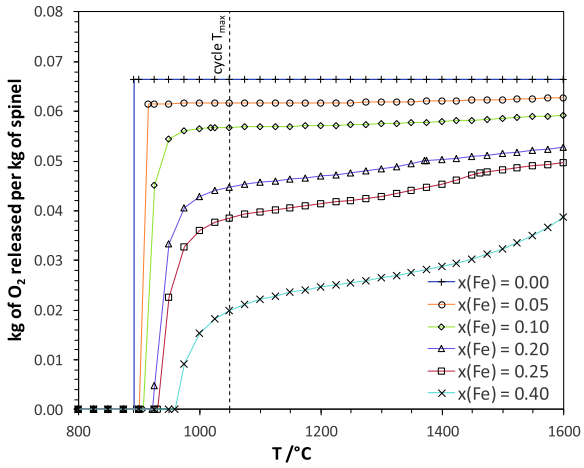

Fig. 8. Temperature evolution of the amount (kg) of O_2(g) released per kg of cobalt-based spinel containing various amounts of Fe.

experimental oxygen partial pressure should be around 10^{-5} atm (10 ppm O_2), which corresponds to a transition temperature of about 650–700 °C but it increases with a higher pO_2. Furthermore, the calculated transition temperature depends noticeably on the composition of the system. It is thus concluded that, with a heating rate of 20 °C/min, the system does not reach equilibrium at low temperature, most likely because of solid-state diffusion limitations. Independently of the system composition, a minimum temperature threshold of about 850 °C is required to achieve the phase transition.

The effect of applying a higher temperature limit than 1050 °C was also estimated, both with experimental measurements and calculations. Cycles with a maximal temperature of 1150 °C were carried out on Co_3O_4 with 5 mol% Fe (Fig. SI7). While this sample behaved well with a maximum temperature set at 1050 °C, the heating up to 1150 °C clearly affected its reactivity. Indeed, the sample did not regain the whole mass on cooling (67% average instead of 86% when heating at 1050 °C) and was sintered at the end of the run.

Furthermore, equilibrium calculations show that applying a temperature limit higher than 1050 °C will not increase drastically the oxygen storage capacity of mixed Co-Fe oxides, as illustrated by Fig. 8. Indeed, for Fe contents between 0% and 10%, the oxygen storage capacity is almost constant with temperature, because the non-stoichiometry of the monoxide is stable. For higher Fe contents ($0.10 < x(Fe) < 0.40$), a small increase of the storage capacity is evidenced at high temperature, due to a higher conversion rate of the spinel phase (Fig. 3b), but Fe addition is still detrimental for the total storage capacity.

As reported in Fig. 9, the measured reaction enthalpies are decreasing with increasing amount of Fe: the highest measured enthalpy is 597 kJ/kg for pure Co_3O_4, while the lowest is 50.7 kJ/kg for x(Fe) = 0.40. It should be noted that the DSC peaks for x(Fe) = 0.40 are very small, which makes them difficult to analyze. For pure Co_3O_4, our data is close to the value of 576 kJ/kg obtained by [2] with a similar experimental procedure. As recently discussed in details by Block et al. [22], this kind of DSC measurements, operated in an open reactor at a rather fast heating rate, is not able to reproduce the tabulated enthalpy value, which is commonly reported as 844 kJ/kg [3–6]. To explain the large discrepancy, the authors state that the contribution of a Co^{3+} spin-state change, associated with an enthalpy of about 222 kJ/kg, is not measured by dynamic techniques.

The thermodynamic model used in this study [13], which takes into account the heat capacity anomaly due to spin-state transition of Co^{3+}, leads to an enthalpy of reaction of 749 kJ/kg for x(Fe) = 0. This is noticeably lower than the commonly admitted value of 827 kJ/mol [2,22]. For higher Fe contents, the calculations reproduce well the general trend (decrease of $\Delta_r H$) with a systematic gap of about 180 kJ/kg.

In TES application, the enthalpy of the reaction is related to the oxygen storage capacity of the material (the energy stored/released during the reduction/oxidation is related to the reaction extent that corresponds to the quantity of O_2 released/captured). As evidenced by measurements and calculations, the gravimetric energy storage density of mixed oxides is decreased when compared with pure Co_3O_4, resulting in less storage capacity per gram of material. This observation is in accordance with the work of Block et al. [2], who stated that both pure Co_3O_4 and Fe_2O_3 show higher enthalpies of reaction than any mixture of the two.

In summary, while the Co_3O_4/CoO redox pair shows very good cycling stability, the addition of iron is shown to slightly affect it and to decrease drastically the overall oxygen storage capacity. According to equilibrium calculations in the Co-Fe-O system, the addition of iron to Co_3O_4 results in a lower amount of O_2 exchanged during cycles and a loss of the reduction reaction enthalpy, due to an incomplete conversion of the spinel phase at 1050 °C and to the formation of a non-stoichiometric monoxide. The addition of iron also increases the reduction and oxidation temperatures, while slightly decreasing the gap in temperature between the reduction and the oxidation step.

3.2. Manganese-based mixed oxides

The calculated Mn-Fe-O phase diagram is presented in Fig. 10, for pO_2 = 0.20 atm. Again, the expected behavior of the mixed oxides is strongly dependent on the system composition. At Fe contents above 50%, the requested temperature to reach a full conversion of the initial oxide into a spinel phase is above 1100 °C. At very low Fe contents ($0 < x(Fe) < 0.05$), the stable phase at 1050 °C is the tetragonal spinel. For $0.05 < x(Fe) < 0.15$, the transition of bixbyite to cubic spinel goes

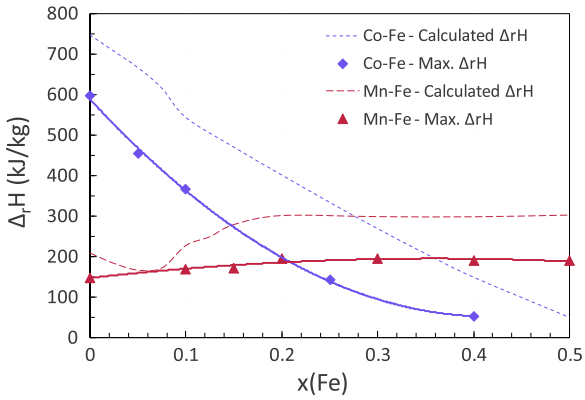

Fig. 9. Experimental and calculated enthalpies of reaction for the Co-Fe and Mn-Fe mixed oxides.

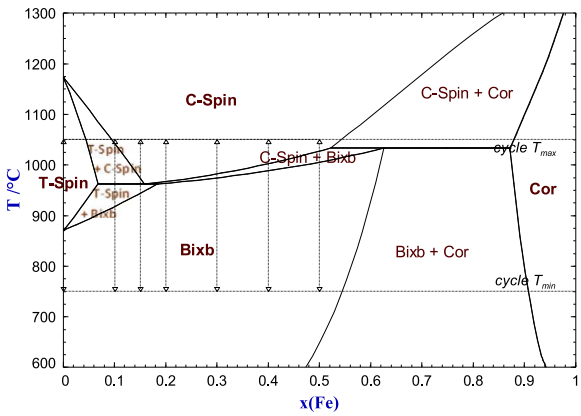

Fig. 10. Calculated Mn-Fe-O phase diagram at pO_2 = 0.20 atm.

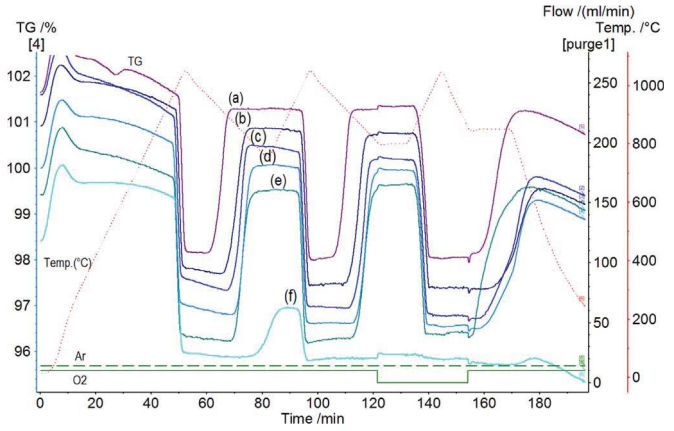

Fig. 11. TGA of Mn_2O_3/Mn_3O_4 with addition of (a) 50 mol% Fe, (b) 40 mol% Fe, (c) 30 mol% Fe, (d) 20 mol% Fe, (e) 15 mol% Fe, and (f) 10 mol% Fe.

through two consecutive two-phase zones (T-Spin+Bixb and T-Spin+C-Spin). Finally, above about 20 mol% Fe, the material transforms almost directly from the bixbyite phase to the cubic spinel.

According to the model [15], the non-stoichiometry of the oxide phases should not play a significant role regarding oxygen storage capacity. Indeed, the bixbyite phase $(Mn_{1-x}Fe_x)_2O_3$ is considered as fully stoichiometric. For the spinel phases T-Spin and C-Spin, a cationic non-stoichiometry is considered in the model, with the presence of cationic vacancies. However, as shown in Fig. SI8, the vacancies concentration at 1050 °C is at the most 1.4×10^{-4} mol per mol of Mn +Fe, which leads to a negligible impact on the oxygen storage capacity. In the composition range $0 < x(Fe) < 0.5$ considered in this study, the redox cycle is thus represented by:

$$(Mn_{1-x}Fe_x)_2O_{3(s)} = 2/3\ (Mn_{1-x}Fe_x)_3O_{4(s)} + 1/6\ O_2(g) \quad (7)$$

At equilibrium, according to the model, the theoretical amount of O_2 exchanged between 750 °C and 1050 °C remains thus the same in the $0 < x(Fe) < 0.5$ composition range.

The TGA, presented in Fig. 11, shows that the sample with the composition x(Fe) = 0.10 is unable to regain its full mass during oxidation, as the mass lost during the first reduction step is not recovered during the re-oxidation step, similarly to the case of pure Mn_2O_3 (TGA shown in Fig. SI9). Conversely, the other compositions, from 15 mol% Fe to 50 mol% Fe, are regaining their lost mass in a complete reversible way. XRD analysis of Mn-Fe samples after TGA was performed (Fig. SI2). The XRD pattern of Mn_2O_3 with 10 mol% Fe is identified as a mixture of tetragonal spinel structure and Fe_2O_3 (Fig. SI2e), which confirms the poor re-oxidation yield of the cycled material. Conversely, the XRD pattern of Mn_2O_3 with 20, 30, 40 and 50 mol% Fe after TGA is identified as $(Mn_{1-x}Fe_x)_2O_3$ (Fig. SI2a–d) with Fe_2O_3 visible on the sample with the highest amount of Fe added (Fig. SI2a), which denotes the complete re-oxidation of the samples after TGA. SEM characterization of the cycled materials compared with the fresh ones reveals sintering regardless of the amount of Fe (Fig. SI10), which does not alter the cycling ability of Mn-Fe mixed oxides. Sintering is thus not the cause of the reactivity loss in the case of pure Mn_2O_3 and Mn_2O_3 mixed with 10 mol% Fe.

Experimental and theoretical mass variations, Δm, were compared. As illustrated in Fig. 12a, all the samples feature the same Δm during the first reduction, in good accordance with the equilibrium calculations summarized by (Eq. (7)). However, pure Mn_2O_3 shows cycling stability issues as already evidenced by [8]. This phenomenon is reflected by the drop of the experimental Δm during 2nd and 3rd cycles, showing a decrease of redox activity with redox cycling. Similarly, Mn_2O_3 mixed with 10 mol% Fe also loses cycling stability, regaining only 31% of its lost mass (Fig. 11f). From x(Fe) = 0.15 to 0.50, a great improvement is evidenced, since the experimental Δm

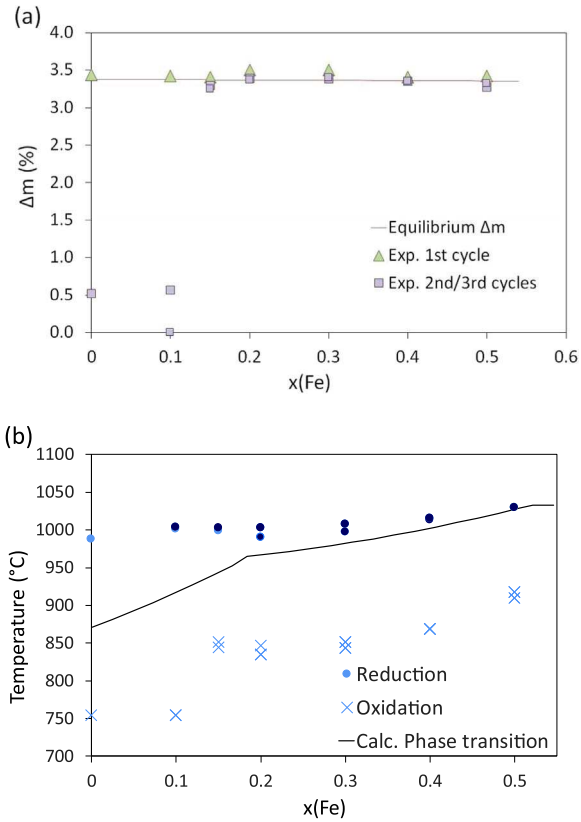

Fig. 12. (a) Evolution of experimental Δm (%) during reduction compared to theoretical Δm (pO_2 = 0.20 atm), (b) Experimental temperatures at peak reaction rate for manganese-based oxides in 20% O_2/Ar and comparison with the calculated temperature of the Bixb/Spinel transition.

value for each cycle remains close both to the maximum Δm value and to the equilibrium value, which denotes negligible deactivation during redox cycling. The addition of iron to Mn_2O_3 thus increases the re-oxidation yield of the material and enhances the cycling stability, as recently observed by Carrillo et al. [11].

Experimental measurements clearly indicate that the minimum Fe content necessary to improve the TES properties of mixed Mn-Fe oxides lies between 10 and 15 mol% Fe. The phase diagram indicates that this corresponds to the formation of the cubic spinel phase only, compared to lower Fe contents, where the tetragonal spinel cannot be reversibly oxidized during cooling. The addition of 20 mol% Fe in Mn_2O_3 was previously mentioned as the optimal composition for obtaining the highest enthalpy and most stable re-oxidation yields [11]. However, the authors also obtained full conversion for all their tested samples regardless of the Fe content (especially below 10% Fe), which contrasts sharply with the results of the present study in which pure Mn_2O_3 and Mn_2O_3 sample with 10 mol% Fe were not able to fully recover the O_2 lost mass. More recently, an in-depth kinetic and mechanistic study focused on the 20 mol% Fe composition was carried out by the same group [23]. It is stated that the cationic distribution in the spinel structures (cubic and tetragonal) might be sufficiently different to explain the strong variation in the kinetics of the oxidation reaction. The use of the thermodynamic model proposed by Kang and Jung [15] brings support to this explanation. Indeed, as illustrated in Fig. 13a, the calculated cationic distribution evidences that the amount of Mn^{2+} on octahedral sites of the spinel strongly increases in the cubic spinel. Furthermore, it has been shown that Mn^{2+} on octahedral sites is easier to oxidize than Mn^{2+} on tetragonal sites [24]. This difference might very well explain the reason why the cycling properties of the cubic spinel are much better than those of the tetragonal spinel.

Another difference between the two spinel structures is that, in the

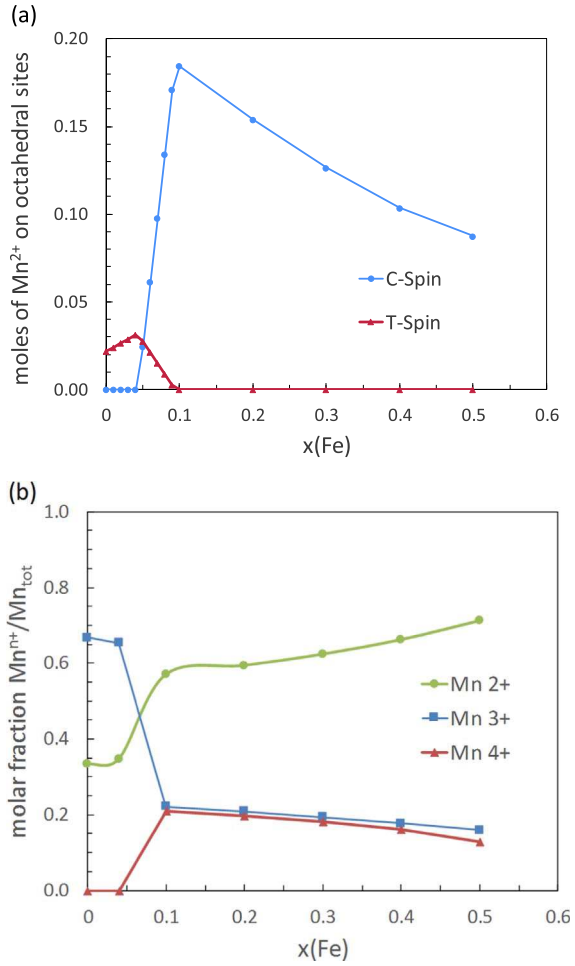

Fig. 13. (a) Evolution of the amount of Mn^{2+} on octahedral sites of the spinel phases with Fe content, at 1050 °C. (b) Evolution of the oxidation number of Mn cations in the spinel phases with Fe content, at 1050 °C.

cubic spinel, a disproportionation reaction takes place according to Mn^{3+}= 1/2 Mn^{4+}+ 1/2 Mn^{2+}, as illustrated in Fig. 13b. The increased amount of Mn^{2+} in the cubic spinel, which can be more easily oxidized than Mn^{3+} thanks to the favored thermodynamic driving force, may also explain the enhanced re-oxidation ability of the cubic spinel. This result means that pure Mn_2O_3 (that reduces into pure tetragonal spinel) and mixed Mn-Fe oxides with Fe content below 15% cannot be suitable candidates for achieving reversible reactions because of the poor re-oxidation ability of the tetragonal spinel formed upon reduction.

As for the influence of Fe incorporation in Mn_2O_3 on the reaction temperatures, a similar tendency as with cobalt oxide is observed. The reduction and oxidation temperatures of Mn_2O_3 softly increase with increasing amount of added iron (Fig. 12b). According to TGA, an increase of 60 °C is noted between the onset temperatures for reduction (Fig. SI11) of pure Mn_2O_3 and Mn_2O_3 with 50 mol% Fe. Concomitantly, a temperature increase of 160 °C is observed for oxidation of Mn_2O_3 with 50 mol% Fe when compared to Mn_2O_3 alone. This way, the reaction temperature can be tuned. On top of an increase of the reaction temperature, addition of iron also reduces the temperature gap between the reduction and the oxidation step. A temperature increase was also reported by [11], with 60 °C difference between 0 and 40 mol% Fe added for the reduction, and 236 °C for the oxidation.

Regarding the effect of the gaseous atmosphere composition, the experimental and theoretical Δm values for the reduction in pure Ar atmosphere were found stable with the addition of Fe to manganese oxide and similar to the Δm measured with 20% O_2. Again, the reduction temperature increases with the O_2 partial pressure (Fig. SI11). The onset temperature for reduction under inert atmosphere rises with the amount of Fe added to manganese oxide, from about 800 °C for pure Mn_2O_3 up to 903 °C for x(Fe) = 0.5 (Fig. SI11). As illustrated by the phase diagram (Fig. SI12) calculated at low pO_2 (10^{-5} atm), decreasing the oxygen content results in enhancing the tetragonal spinel stability, which is likely to be detrimental to the cycling stability of the materials.

As for the energy storage density, the measured enthalpy for the first reduction step with full conversion of pure Mn_2O_3 (148 kJ/kg) is smaller than theoretical estimations of 190.1 kJ/kg at turning temperature (ΔG° = 0) of 915 °C [10]. An average of 187.7 kJ/kg is measured for the samples with compositions between 20 and 50 mol% Fe. Increasing the amount of Fe thus slightly improves the energy storage capacity of the material at low Fe contents while it remains unchanged above ~20 mol% Fe (Fig. 9). Accordingly, the thermodynamic calculations indicate that an increase of $\Delta_r H$ is expected when the Fe content increases from 0 mol% (207 kJ/kg) to 20 mol% (300 kJ/kg), and is stable for higher Fe contents.

In summary, the addition of iron to manganese oxide enhances considerably the cycling stability of the material by improving the re-oxidation yield thanks to the formation of a reactive cubic spinel phase. Also, the higher the amount of Fe added to Mn_2O_3, the higher the reaction temperatures. In addition, the gap in temperature between the reduction and the oxidation decreases with higher iron content. The low re-oxidation yield observed for pure Mn_2O_3 and Mn_2O_3 with 10 mol% Fe is attributed to the low reactivity of the tetragonal spinel phase. The addition of Fe to Mn_2O_3 becomes effective for the enhancement of the cycling stability above ~15 mol% Fe, with the suppression of any transition involving this tetragonal spinel phase. The markedly improved reactivity of the cubic spinel featuring reversible reactions is attributed to the increased amount of Mn^{2+} cations (resulting from Mn^{3+} disproportionation) on octahedral sites of the spinel.

4. Conclusion

The effect of Fe addition in Co and Mn-based oxides was studied experimentally and results were compared with thermodynamic calculations. The calculations were shown to be pertinent since equilibrium is reached at least on the first reduction step of all materials considered in this study. The addition of Fe to Mn_2O_3 was shown to be beneficial to tune the temperature of redox reactions, to reduce the gap in temperature hysteresis between the reduction and the oxidation step, as well as to enhance the re-oxidation kinetics and cycling stability of the material by countering the deactivation issue of Mn_2O_3. Furthermore, a Fe content of ~15 mol% added to Mn_2O_3 was identified as a minimum threshold for avoiding the formation of a low reactive Mn_3O_4 tetragonal spinel phase during reduction, which is detrimental to the reaction reversibility because of poor oxidation rate and yield. Noticeably, the Mn_2O_3 compounds with Fe content in the range 15–50 mol% could be cycled between bixbyite and cubic spinel phases without any reactivity losses during redox reactions. Conversely, the incorporation of Fe to Co_3O_4 shows adverse effect on the redox performances since both the maximum amount of O_2 exchanged and the reaction enthalpy are lowered when the amount of iron added is increased. The increasing amount of iron added to Co_3O_4 reduces the maximum oxygen exchange capacity during a redox cycle. The addition of iron to Co and Mn-based oxides also results in an increase of the reaction temperatures, while slightly lowering the gap in temperature between the reduction and oxidation step, which thereby reduces the sensible energy losses during the heating and cooling stages. The comparison of the obtained experimental data with thermodynamic modelling proves that equilibrium calculations bring a strong support for predicting the behavior of mixed oxides since it results in consistent

phase transition temperatures and reliable oxygen storage capacities. It further provided new physical insights into the role of Fe incorporation on the oxidation improvement of Co and Mn-based oxides related to the crystallographic transformations that take place during such redox process depending on Fe content. With the development of new models covering large multi-components systems, it could be further used for selecting other transition metals to enhance the properties of mixed metal oxides for thermochemical energy storage application.

Acknowledgments

This study was performed in the framework of the STAGE-STE European Project (FP7, Project no. 609837). Philippe Tailhades is warmly thanked for the fruitful discussion on spinel properties.

Appendix A. Supplementary material

Supplementary data associated with this article can be found in the online version at doi:10.1016/j.jssc.2017.05.015.

References

[1] A.H. Abedin, M.A. Rosen, A critical review of thermochemical energy storage systems, Open Renew. Energy J. 4 (2011) 42–46.
[2] T. Block, N. Knoblauch, M. Shmücker, The cobalt-oxide/iron-oxide binary system for use as high temperature thermochemical energy storage material, Thermochim. Acta 577 (2014) 25–32.
[3] C. Agrafiotis, M. Roeb, M. Schücker, C. Sattler, Exploitation of thermochemical cycles based on solid oxide redox systems for thermochemical storage of solar heat. Part 2: redox oxide-coated porous ceramic structures as integrated thermochemical reactors/heat exchangers, Sol. Energy 114 (2015) 440–458.
[4] C. Agrafiotis, S. Tescari, M. Roeb, M. Schücker, C. Sattler, Exploitation of thermochemical cycles based on solid oxide redox systems for thermochemical storage of solar heat. Part 3: cobalt oxide monolithic porous structures as integrated thermochemical reactors/heat exchanger, Sol. Energy 114 (2015) 459–475.
[5] M. Neises, S. Tescari, L. De Oliveira, M. Roeb, C. Sattler, B. Wong, Solar-heated rotary kiln for thermochemical energy storage, Sol. Energy 86 (2012) 3040–3048.
[6] S. Tescari, C. Agrafiotis, S. Breuer, L. De Oliveira, M. Nieses-von Puttkamer, M. Roeb, C. Sattler, Thermochemical solar energy storage via redox oxides: materials and reactor/heat exchanger concepts, Energy Procedia 49 (2014) 1034–1043.
[7] G. Karagiannakis, C. Pagkoura, A. Zygogianni, S. Lorentzou, A.G. Konstandopoulos, Monolithic ceramic redox materials for thermochemical heat storage applications in CSP plants, Energy Procedia 49 (2014) 820–829.
[8] A.J. Carrillo, D.P. Serrano, P. Pizarro, J.M. Coronado, Improving the thermochemical energy storage performance of the Mn_2O_3/Mn_3O_4 redox couple by the incorporation of iron, ChemSusChem 8 (2015) 1947–1954.
[9] C. Pagkoura, G. Karagiannakis, A. Zygogianni, S. Lorentzou, M. Kostoglou, A.G. Konstandopoulos, M. Rattenburry, W.J. Woodhead, Cobalt oxide based structured bodies as redox thermochemical heat storage medium for future CSP plants, Sol. Energy 108 (2014) 146–163.
[10] L. André, S. Abanades, G. Flamant, Screening of thermochemical systems based on solid-gas reversible reactions for high temperature solar thermal energy storage, Renew. Sustain. Energy Rev. 64 (2016) 703–715.
[11] A.J. Carrillo, D.P. Serrano, P. Pizarro, J.M. Coronado, Thermochemical heat storage based on the Mn_2O_3/Mn_3O_4 redox couple: influence of the initial particle size on the morphological evolution and cyclability, J. Mater. Chem. A 2 (2014) 19435–19443.
[12] A.J. Carrillo, D.P. Serrano, P. Pizarro, J.M. Coronado, Manganese oxide-based thermochemical energy storage: modulating temperatures of redox cycles by Fe-Cu Co-doping, J. Energy Storage 5 (2016) 169–176.
[13] I.H. Jung, S.A. Decterov, A.D. Pelton, H.M. Kim, Y.B. Kang, Thermodynamic evaluation and modeling of the Fe-Co-O system, Acta Mater. 52 (2004) 507–519.
[14] W.-W. Zhang, M. Chen, Thermodynamic modeling of the Co–Fe–O system, Calphad 41 (2013) 76–88.
[15] Y.B. Kang, I.H. Jung, Thermodynamic modeling of oxide phases in the Fe-Mn-O system, J. Phys. Chem. Solids 98 (2016) 237–246.
[16] L. Kjellqvist, M. Selleby, Thermodynamic assessment of the Fe-Mn-O system, J. Phase Equilib. Diffus. 31 (2010) 113–134.
[17] E. Beche, G. Peraudeau, V. Flaud, D. Perarnau, XPS unvestigation of $(La_2O_3)_{1-x}$ $(CeO_2)_{2x}$ $(ZrO_2)_2$ compounds elaborated by solar energy, Surf. Interface Anal. 44 (2012) 1045–1050.
[18] J.i. Lai, K.V.P.M. Shafi, A. Ulman, N.-L. Yang, M.-H. Cui, T. Vogt, C. Estournès, Mixed iron-manganese oxide nanoparticles, Nanopart. Chem. Soc. Div. Fuel Chem. 48 (2) (2003) 729–730.
[19] C.W. Bale, E. Bélisle, P. Chartrand, S.A. Decterov, G. Eriksson, A.E. Gheribi, K. Hack, I.H. Jung, Y.B. Kang, J. Melançon, A.D. Pelton, S. Petersen, C. Robelin, J. Sangster, P. Spencer, M.A. Van Ende, FactSage thermochemical software and databases, 2010–2016, Calphad 54 (2016) 35–53.
[20] M. Hillert, The compound energy formalism, J. Alloy. Compd. 320 (2) (2001) 161–176.
[21] B. Ehrhart, E. Coker, N. Siegel, A. Weimer, Thermochemical cycle of a mixed oxide for augmentation of thermal energy storage in solid particles, Energy Procedia 49 (2014) 762–771.
[22] T. Block, M. Schmucker, Metal oxides for thermochemical energy storage: a comparison of several metal oxide systems, Sol. Energy 126 (2016) 195–207.
[23] A.J. Carrillo, D.P. Serrano, P. Pizarro, J.M. Coronado, Understanding redox kinetics of iron-doped manganese oxides for high temperature thermochemical energy storage, J. Phys. Chem. C 120 (2016) 27800–27812.
[24] F. Agnoli, B. Albouy, P. Tailhades, A. Rousset, Manganites de Fer de Structure Spinelle Déformée à Très Fort Champ Coercitif. Exemple de l'Oxyde Lacunaire Mixte $Mn_{1.7}Fe_{1.3}O_{4+\delta}$, C. R. Acad. Sci. 2 (1999) 525–530.